Tellus (1991), *43B*, 301–321

The scavenging of two different types of marine aerosol particles calculated using a two-dimensional detailed cloud model

By ANDREA I. FLOSSMANN, *Institute for Atmospheric Physics, Johannes Gutenberg University, D-6500 Mainz, Germany*

(Manuscript received 28 March 1990; in final form 19 November 1990)

ABSTRACT

Our 2-D dynamic model including spectral microphysics and scavenging has been evaluated for a warm precipitating convective cloud at Day 261 (18 September 1974) of the GATE campaign. Two different chemical species ($(NH_4)_2SO_4$ and NaCl) of aerosol particles were followed in the air, inside the drops in the cloud, and inside the drops reaching the ground. Concerning the dynamics and microphysics, as well as the scavenging and wet deposition, the model results agree quite well with available observations. The cloud rained after 19 min of cloud life time. For the considered aerosol loading of the atmosphere, rough estimates are derived for the total material processed by such a warm convective cloud as input for larger scale models. In particular, the following conclusions could be drawn for the situation considered. (1) If a drop spectrum forms on an aerosol spectrum where the small particles consist of $(NH_4)_2SO_4$ and the large ones of NaCl, the resulting small drops also mainly consist of $(NH_4)_2SO_4$ and the larger drops of NaCl. Collision and coalescence causes a redistribution of the chemical species such that the precipitation sized drops consist of NaCl to about 70%. (2) The mixing ratio of aerosol material in the drops is a function of the age of the drops and their history and therefore the variation of the mixing ratio with drop size depends on the entrainment and evoluion of the relative humidity. The mixing ratio decreased with increasing drop radius at almost all grid points due to continuous activation of fresh particles. (3) Assuming that the sulfate aerosol would not consist of $(NH_4)_2SO_4$ particles but instead consist of NH_4HSO_4 particles the acidic cloud water has a pH of 4.7 which agrees with observations of marine precipitation. (4) The scavenging efficiency of the cloud considered is closely related to its precipitation efficiency (both near 40%). About 90% of the total amount of aerosol material scavenged is incorporated into the cloud water through nucleation scavenging. About 30% of the aerosol material in the rain at the ground is due to scavenging below cloud base. (5) The scavenging coefficient of the considered storm was on the order of 10^{-4} s^{-1}. Differences between two commonly used formulations for calculating the scavenging coefficient Λ can be explained in terms of humidity changes of the atmosphere.

1. Introduction

Wet removal by clouds and precipitation plays an important role in determining the distribution and concentration of pollutants in the atmosphere. In addition it is the cause for the acidity found in rainwater which has considerable impact on the environment. In order to study the mechanism underlying the wet removal and the consequent loading of cloud and rainwater with pollutants several approaches have been followed in literature.

On the one hand, field studies have been performed to address various aspects of this problem. Thus, the variation of the chemical composition in the cloud and rainwater has been monitored by Scott and Laulainen (1979), Hegg and Hobbs (1982), Kins (1982), Lazrus et al. (1983), Leaitch et al. (1983), Murakami et al. (1983), Schumann et al. (1988), and Ogren et al. (1989), among others. The aerosol in the air in between the cloud drops has been studied by Radke (1983), and Daum et al. (1983). Since most clouds develop in a rather complex manner, involving the liquid as

well as the ice phase, and scavenge a variety of different particles and gases, field experiments are difficult to interpret with respect to the active scavenging mechanisms.

On the other hand, modeling studies have been performed using a variety of different model dynamics. Unfortunately, the treatment of the microphysics as well as the scavenging mechanism in these models varies greatly, ranging from a very detailed approach to highly parametrized formulas. For a review of some recent modeling approaches see Flossmann and Pruppacher (1988). This review shows that most models lack realism from numerous points of view or have not been applied to realistic scenarios. In particular, they have, thus far, not considered the fact that chemically the atmospheric aerosol consists of an external mixture of particles each of which represents an internal chemical mixture. In addition, small particles often have a different composition than larger ones. An exception to this are the models of Twohy et al. (1989) and Ayers and Larson (1990) which have calculated the diffusional growth of cloud droplets on a marine aerosol spectrum consisting of sulfate and sea salt particles. However, they did their calculation in the simple dynamics of an ascending air parcel and neglected all other microphysical processes.

In an attempt to take into account the above-mentioned neglect in the chemical details of the scavenged aerosol and to consider a realistic warm rain scenario, we have applied our spectral microphysical and scavenging model embedded in a two-dimensional framework (Flossmann et al., 1985; Flossmann and Pruppacher, 1988) to the scavenging of the two major types of aerosol particle (NaCl and $(NH_4)_2SO_4$) as they are found in marine air masses. Consequently, the Hawaiian situation, modelled in Flossmann and Pruppacher (1988), could not be used, since those clouds originate on an aerosol particle spectrum influenced by the land. Thus, we applied our model to air over the Atlantic Ocean where warm rain clouds formed on the Day 261 (18 September 1974) during the GARP Atlantic Tropical Experiment (GATE) at 9° N 23° W. The conditions during that campaign period were particularly suitable for this research because of the prevalence of relatively small shower clouds in which the ice phase played no role. Also the meteorological situation was fairly well documented (Turpeinen and Yau, 1981; WMO Report, 1986). Therefore, Day 261 has already been used as input for simulations, e.g. by Turpeinen and Yau (1981), and Simpson et al. (1982), which reproduced the observed dynamics fairly well due to the three dimensionality of their models, which, however contained a heavily parameterized representation of cloud microphysics.

Unfortunately, no scavenging information was available for the GATE campaign. However, the aerosol particle size distribution as well as the chemical composition of marine air masses have been fairly well documented by Jaenicke (1988), and Parungo et al. (1986a, b), among others. Thus, we assumed the maritime aerosol particle spectrum given by Jaenicke (1988) with the large particles consisting of NaCl and the smaller ones to be $(NH_4)_2SO_4$. Both species were assumed to decrease with height whereby it was taken into account that NaCl is confined to below 2.5 km. In addition, Parungo et al. (1986b) measured the chemical composition of rain water at a location close to that of the GATE campaign, although a few years later.

In contrast to our earlier spectral models (Flossmann et al., 1985; Flossmann and Pruppacher, 1988; Ahr et al., 1990) where only the *total mass of aerosol material* inside the drops was considered, we reformulated our model such that *each of the two chemical species of scavenged aerosol particles* could be followed inside the drops of a given size class as the cloud developed. This additional model detail allowed us to determine differences in the uptake and deposition rate of the two chemical species.

2. The present model

As discussed in detail by Flossmann and Pruppacher (1988) the basic dynamic framework employed in the present study is a two-dimensional slab-symmetric version of the three-dimensional model which has been described, e.g., by Clark (1977, 1979), Clark and Gall (1982), Clark and Farley (1984), and Hall (1980). For the sake of brevity only the model features which differ from those of Flossmann and Pruppacher (1988) or deal with the newly considered two species of aerosol particles are given below.

The time rate of change of the cloud drop

number density distribution function f_d is given by the relation

$$\frac{\partial f_d(m)}{\partial t} = -\nabla \cdot [\boldsymbol{v} f_d(m)] + \nabla \cdot [K_m \nabla f_d(m)] + \frac{\partial}{\partial z}[V_\infty(m)\, f_d(m)] + \left.\frac{\partial f_d(m)}{\partial t}\right|_{act} + \left.\frac{\partial f_d(m)}{\partial t}\right|_{con/eva} + \left.\frac{\partial f_d(m)}{\partial t}\right|_{AP,coll} + \left.\frac{\partial f_d(m)}{\partial t}\right|_{d,coal} + \left.\frac{\partial f_d(m)}{\partial t}\right|_{d,break}. \quad (1)$$

The time rate of change of the number density distribution function for $(NH_4)_2SO_4$ particles and NaCl particles, resp., remaining in the air, f_{APa}, is given by:

$$\frac{\partial f_{APa}(m_{AP})}{\partial t} = -\nabla \cdot [\boldsymbol{v} f_{APa}(m_{AP})] + \nabla \cdot [K_m \nabla f_{APa}(m_{AP})] + \left.\frac{\partial f_{APa}(m_{AP})}{\partial t}\right|_{act} + \left.\frac{\partial f_{APa}(m_{AP})}{\partial t}\right|_{con/eva} + \left.\frac{\partial f_{APa}(m_{AP})}{\partial t}\right|_{AP,coll}. \quad (2)$$

The time rate of change of the mass density distribution function of $(NH_4)_2SO_4$ particles and NaCl particles, respectively, in the drops, g_{APd}, is given by

$$\frac{\partial g_{APd}(m)}{\partial t} = -\nabla \cdot [\boldsymbol{v} g_{APd}(m)] + \nabla \cdot [K_m \nabla g_{APd}(m)] + \frac{\partial}{\partial z}[V_\infty(m)\, g_{APd}(m)] + \left.\frac{\partial g_{APd}(m)}{\partial t}\right|_{act} + \left.\frac{\partial g_{APd}(m)}{\partial t}\right|_{con/eva} + \left.\frac{\partial g_{APd}(m)}{\partial t}\right|_{AP,coll} + \left.\frac{\partial g_{APd}(m)}{\partial t}\right|_{d,coal} + \left.\frac{\partial g_{APd}(m)}{\partial t}\right|_{d,break}, \quad (3)$$

and the time rate of change of the mass density distribution function for the $(NH_4)_2SO_4$ particles and NaCl particles, resp., remaining in the air, g_{APa}, is given by

$$\frac{\partial g_{APa}(m_{AP})}{\partial t} = -\nabla \cdot [\boldsymbol{v} g_{APa}(m_{AP})] + \nabla \cdot [K_m \nabla g_{APa}(m_{AP})] + \left.\frac{\partial g_{APa}(m_{AP})}{\partial t}\right|_{act} + \left.\frac{\partial g_{APa}(m_{AP})}{\partial t}\right|_{con/eva} + \left.\frac{\partial g_{APa}(m_{AP})}{\partial t}\right|_{AP,coll}, \quad (4)$$

where m = mass of drop, m_{AP} = mass of aerosol particle, $\boldsymbol{v}$ = velocity field of air, ψ = time rate of change of the functions f_d, g_{APd}, f_{APa}, g_{APa}. $\psi|_{act}$ = change due to activation of aerosol particles to drops (nucleation scavenging), $\psi|_{con/eva}$ = change due to condensation and/or evaporation of drops, $\psi|_{AP,coll}$ = change due to aerosol particle collection (impaction scavenging), $\psi|_{d,coal}$ = change due to collision and coalescence of drops, $\psi|_{d,break}$ = change due to drop break up.

The first three terms in eqs. (1) and (3) and the first two terms in eqs. (2) and (4) were evaluated from the dynamic framework of the two-dimensional cloud dynamics model as described in Flossmann and Pruppacher (1988). The remaining microphysical terms were evaluated following Flossmann et al. (1985) and Flossmann (1987). For the extensive bookkeeping in order to follow the uptake and redistribution of the two chemical species considered the development of a special numerical code was necessary.

3. Initial conditions and description of heating source

The present model was initialized with a warm cloud sounding taken at Day 261 (18 September 1974) of the GATE campaign at 12 GMT. Our 2-D model domain was oriented in the north-south, as this was the main wind direction. Therefore, the sounding used in the model (Fig. 1) was a combination of the one analyzed by Turpeinen and Yau (1981) and the model data set available from the WMO (WMO Report, 1986). In the lower 2 km the wind was southerly as well as above 6 km. In between the wind was northerly.

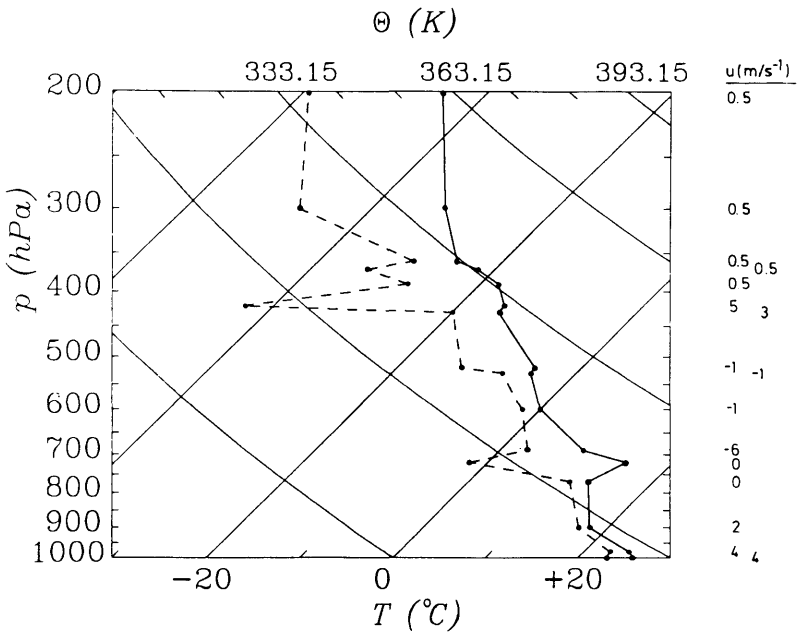

Fig. 1. Sounding of GATE 261 as used in model calculation.

As for this special campaign no field observations on the prevailing aerosol were available, we assumed a maritime aerosol particle size spectrum consisting of a superposition of three log-normal distributions as suggested by Jaenicke (1988) which resulted from a compilation of numerous observed spectra. This size distribution agrees well with the spectra measured by Parungo et al. (1986b) during a ship cruise over the Atlantic Ocean passing through the GATE observation domain. Mode 1 and mode 2 were assumed to consist of $(NH_4)_2SO_4$ or alternatively, for the estimate of a pH, of the acidic NH_4HSO_4 and were combined in one number density distribution function

$$\frac{dN_{APa}}{d\ln r_N} = f_{APa}(\ln r_N)$$

$$= \sum_{i=1}^{2} f_{APa,i}(\ln r_N)$$

$$= \sum_{i=1}^{2} \frac{n_i}{(2\pi)^{1/2}\log\sigma_i \ln 10} \times \exp\left(-\frac{[\log(r_N/R_i)]^2}{2(\log\sigma_i)^2}\right), \quad (5)$$

while the third mode was set to be NaCl:

$$\frac{dN_{APa}}{d\ln r_N} = f_{APa}(\ln r_N)$$

$$= \frac{n_3}{(2\pi)^{1/2}\log\sigma_3 \ln 10} \times \exp\left(-\frac{[\log(r_N/R_3)]^2}{2(\log\sigma_3)^2}\right), \quad (6)$$

where r_N is the radius of the "dry" aerosol particle, R_i is the geometric mean radius by number, n_i the aerosol particle number concentration and σ_i the standard deviation of the ith log-normal distribution. N_{APa} is the total particle concentration in air, and f_{APa} is the number density distribution function for ammonium sulfate or sodium chloride aerosol particles in air, respectively. The parameters n_i, R_i, and σ_i for the maritime aerosol spectrum considered were assumed to have the values given in Table 1 (see Jaenicke, 1988), leading to the number density and volume density distributions, and the CCN spectrum as given in Fig. 2. The number and mass concentration for the two chemical species alone and the total values are

Table 1. *Parameters for the maritime aerosol particle distribution as given in Eqs. (5) and (6); n_i = total number of aerosol particles per cm^3, R_i = geometric mean aerosol particle radius in μm, σ_i = standard deviation in mode i; chemical composition and scale height H_i of the aerosol particle modes*

Mode i	n_i	R_i	$\log \sigma_i$	Chemical compound	H_i(m)
1	133	0.0039	0.657	$(NH_4)_2SO_4$	3000
2	66.6	0.1330	0.210	$(NH_4)_2SO_4$	3000
3	3.06	0.2900	0.396	NaCl	1000

in agreement with observations although literature shows a large spread of values observed. For sea salt Jaenicke (1988) reports on the basis of measurements by Blanchard and Woodcock (1980) 10 to 30 μg/m^3 for wind speeds of 8 m/s. Varhelyi and Gravenhorst (1983) reported for 10.4 m/s 18.5 μg/m^3 as annual average, Prodi et al. (1983) reported for windspeeds of 5 to 10 m/s 10 to 20 μg/m^3, and Lovett (1978) reported 9.5 μg/m^3 for 5m/s, 20 μg/m^3 for 10 m/s and 55 μg/m^3 for 15 m/s. For sulfate on the basis of $(NH_4)_2SO_4$ Varhelyi and Gravenhorst (1983) reported 3.2 μg/m^3, Parungo et al. (1986a) 3.4 μg/m^3 and Wolff et al. (1986) 0.17 to 10.8 μg/m^3 with an average of 5.6 μg/m^3. In addition to these observation also lower values for the marine NaCl and $(NH_4)_2SO_4$ concentrations are certainly possible. We decided, however, to use the distribution suggested by Jaenicke because its analytical form allows an easy application to our considered size range and size intervals. In addition, the three modes underlying the distribution allow to attribute the two smaller modes to $(NH_4)_2SO_4$ and the larger one to NaCl. However, we are aware of the fact that mode 1 extends masswise in a size range which should be reserved for the NaCl particles. The mass associated with this mode, however, is so small that this does not effect the results, neither for in-cloud nor for below-cloud scavenging.

We also assumed that the initial aerosol size

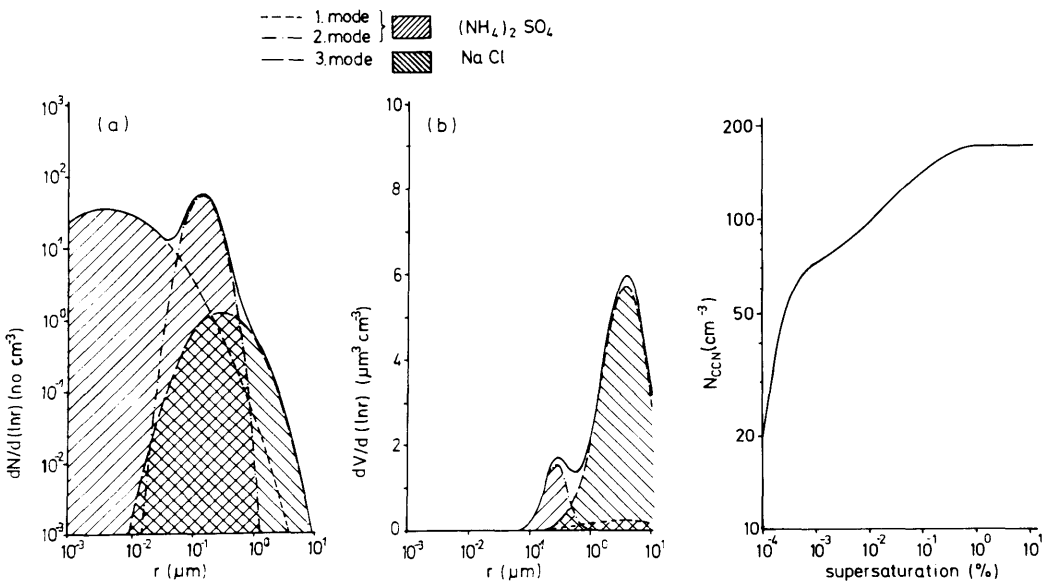

Fig. 2. Number density (a) and volume density (b) distribution and CCN spectrum (c) for aerosol particles of maritime type; the curve for $(NH_4)_2SO_4$ results from the superposition of the modes 1 and 2 in Table 1; $N_{APa}((NH_4)_2SO_4) = 170$ cm^{-3}, $w_{APa}((NH_4)_2SO_4) = 5.5$ μg m^{-3}; the curve for NaCl is represented by the third mode in Table 1; $N_{APa}(NaCl) = 3$ cm^{-3}, $w_{APa}(NaCl) = 24.4$ μg m^{-3}; total number concentration $N_{APa} = 173$ cm^{-3}, and total particle mass $w_{APa} = 30$ μg m^{-3} (in the considered aerosol particle size range between 0.97 10^{-3} μm and 10.08 μm).

distributions decreased with height in the atmosphere according to

$$f_{\mathrm{APa},i}(z) = f_{\mathrm{APa},i}(z=0)\, e^{-z/H_i}, \tag{7}$$

where H_i is given in Table 1.

In order to simplify the calculations the specific gravity of these aerosol particles was assumed to be 2.0 g cm^{-3}. From the size distribution of the dry aerosol particles (eqs. (5), (6)), we computed the initial size distribution for the moist aerosol particles by allowing the dry particles to grow to their equilibrium size at the initial local relative humidity at every grid point of the domain.

The present model covered a domain of 10 km in the vertical and 20 km in the horizontal. The grid spacings were $\Delta z = 200$ m and $\Delta x = 400$ m resulting in 52 by 52 grid points, and the time step was $\Delta t = 5$ s. These grid spacings were chosen in order to keep the numerical expenses within limits. However, they do not allow to resolve in great detail the mixing of environmental air into the cloud at its boundaries. This mixing is highly inhomogeneous, as pointed out by Baker et al. (1980), Baker and Latham (1982), and Hill and Choularton (1986). In our model, however, a homogeneous mixing with a turbulent eddy mixing coefficient K_m according to the first order theory of Smagorinsky (1963) and Lilly (1962) is assumed. This might influence the scavenging properties at the cloud edges and will be a subject of future investigations.

The dynamic model of Clark et al. which we used for our model study is driven by a sensible and latent heat flux from the surface as formulated by Clark and Gall (1982) and by a parameterized version of the detailed calculations of Smolarkiewicz and Clark (1985) as described in Flossmann and Pruppacher (1988). In the present calculation the average surface sensible heat flux P_H was assumed to be 30%, and the latent heat flux P_Q to be 2% of the incoming solar flux. These fluxes are assumed to consist of a background heat flux and a Gaussian perturbation fraction where it was assumed that the fraction of the total energy which goes into the Gaussian perturbation of the sensible heat flux was $\beta_H = 60\%$, and the fraction that goes into the Gaussian perturbation of the latent heat flux was $\beta_Q = 0.1\%$, and where it was assumed that the half width of the Gaussian perturbation was $\sigma_H = 3600$ m and $\sigma_Q = 3600$ m. The selected values are in agreement with observations reported by Clark and Gall (1982). The coordinate x_0 locates the maximum of heating at 7 km so that the main cloud stays inside the considered domain during the computations. These heat and moisture sources were assumed to have their maximum value at the ground and attenuate exponentially with height so that at 150 m they had decreased in strength to 1/e of their surface value. The heating source was turned off after 30 min when the cloud formed. This was done to account for the shading effect of the cloud.

The complete composite model was evaluated on the CRAY X-MP/216 at the DLR Oberpfaffenhofen, FRG. The model run took 3 h of computer time.

4. Results and discussion

The calculations started at 12 GMT. The surface sensible and latent heat flux caused the air to rise and after 26 min of model time a cloud had formed at $x = 11$ km. The situation after 30 min where the cloud is 4 min old is displayed in Fig. 3. Note the warming of the air due to heat flux from the ground in Fig. 3a. The relative humidity in Fig. 3b has a local maximum of 100.54% at around $x = 11.5$ km. The displacement from the maximum heating at 7 km is due to the horizontal wind shear. The region of supersaturation corresponds to the field of liquid water which is displayed in Fig. 3c. It's maximum, however, is quite small (0.2 g/kg) as the cloud is just 4 min old. Cloud base is located at 800 m and cloud top at 1400 m. The diameter of the cloud is 2.4 km. These dimensions are caused by the width of the grid spacing intervals $\Delta x = 400$ m and $\Delta z = 200$ m. The vertical grid spacing also does not allow to resolve explicitly the reported peek in the supersaturation only a few meters above cloud base (see, e.g., Ahr et al., 1990). However, the calculated supersaturations at cloud base for this dynamical case with strong updrafts are always larger than 0.3%. The CCN spectrum displayed in Fig. 2c shows that for this supersaturation almost all available CCN of this marine aerosol particle spectrum are already activated. Thus, the inadequate resolution of the peek supersaturation at cloud base does only underpredict the number of CCN by a few particles. The effects on the nucleated aerosol mass is even smaller since

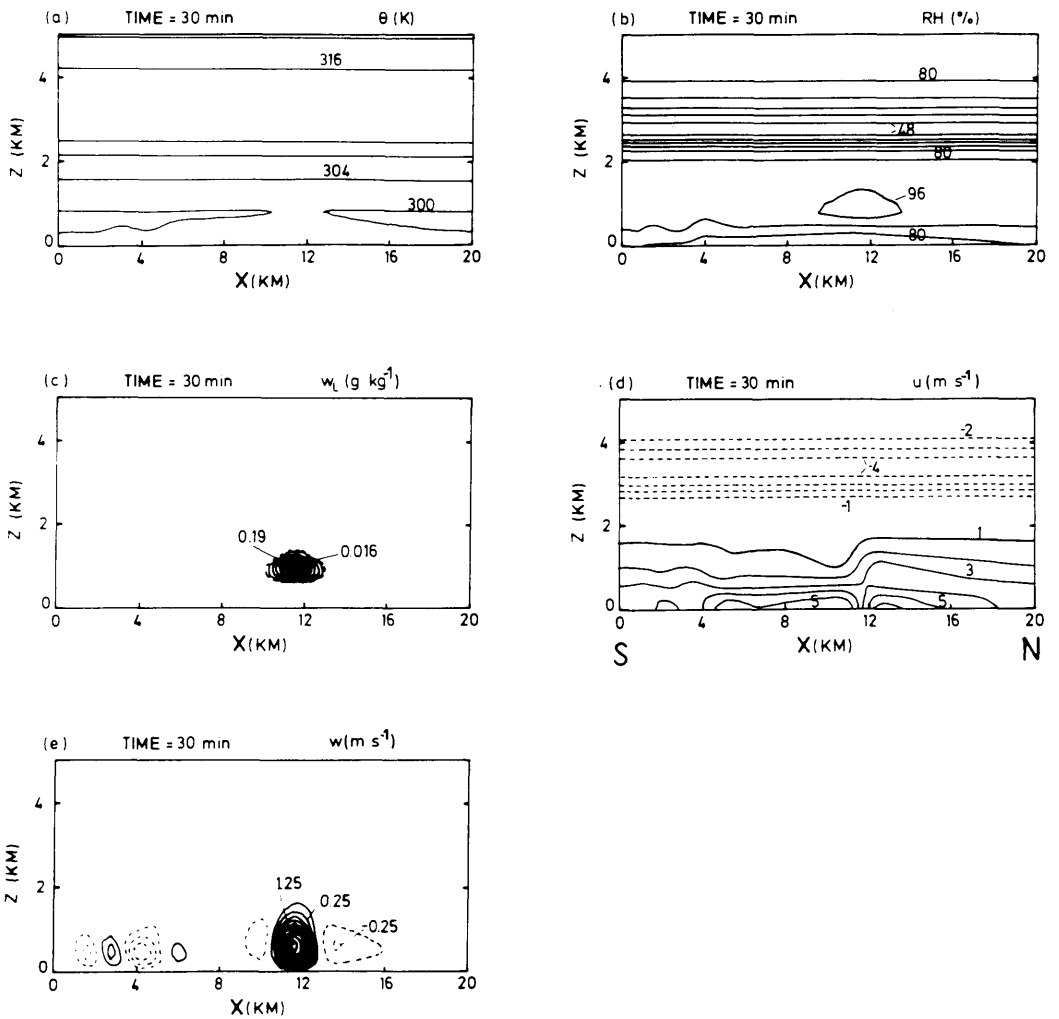

Fig. 3. Distribution of (a) θ, (b) RH, (c) w_L, (d) u, and (e) w inside domain at model time $t = 30$ min (corresponds to 4 min after the first cloud formed); with the contour intervals: $\Delta\theta = 4$ K, $\Delta RH = 8\%$, $\Delta w_L = 0.0016$ g/kg, $\Delta u = 1$ m/s, $\Delta w = 0.125$ m/s.

these particles are quite small. In Fig. 3d where the horizontal wind speed u is given we notice the southerly winds in the lower 2 km which already are disturbed due to the developing convection cell. The northerly flow aloft is not influenced by the circulation. In Fig. 3e for the vertical wind speed w we notice the ascending air around 11 km belonging to the main convection cell and around 3 and 6 km secondary cells begin to develop. In order not to overcomplicate things we will only discuss the main large cell and disregard the secondary small cells forming on the left hand side of the domain.

As time increases, the main cell gets larger and the originally small drops grow through condensation to larger sizes. Subsequently, collision and coalescence form large drops which after 14 min (40 min of model time) begin to leave cloud base and fall towards the ground. After 19 min (45 min of model time) the rain has reached the ground. This relatively fast onset of precipitation at first might seem surprising since common textbooks

still claim that due to condensational growth of the droplets the spectrum stays too narrow for collision and coalescence to become important. Only the inhomogeneous mixing would sufficiently broaden the spectrum for rain to form. But mixing only occurs at the very edges of the cloud and precipitation sized drops form also deep inside the cloud. In order to shed light on this problem we studied with a parcel model the process of rain initiation (Roesner et al., 1990) and found that precipitation sized drops form within a reasonable time if the collision and coalescence process was considered at all times and not just turned on once the spectrum becomes broad enough. Even though the collision and coalescence process is small while the drop spectrum is narrow, it still produces few large drops which then help to initiate rain formation.

The situation after 50 min of model time (24 min of cloud time) is displayed in Figs. 4 and 5. Fig. 4 shows the distribution of (a) θ, (b) RH, (c) u, and (d) w. In Fig. 4b, we notice 5 regions associated with supersaturation. The three at the left hand side of the domain belong to the developing secondary cells while the two others belong to the main cell. Originally this was one big cell but the downdrafts associated with the rainfall have cut the cell into two. The right one is the more vigorous one and moves ahead with the southerly flow. The left cell stays in place and dies. This is also reflected in Fig. 5a for the total liquid water content and in Fig. 5b for the liquid water content in the drops smaller than 30 μm. This figure illustrates the contours of the visible cloud. Here cloud base is at 800 m and cloud top is at 3000 m. The amounts of scavenged $(NH_4)_2SO_4$ and NaCl in the cloud water are displayed in Figs. 5c and d, respectively. Notice that the main aerosol mass is associated with the main water mass as already suggested by Flossmann and Pruppacher (1988). Figs. 5e, f display the corresponding reduction in the aerosol particle mass in the air. This reduction is most pronounced inside the cloud domain where the air is supersaturated (see Fig. 4b), as there nucleation scavenging is consuming over 90% of the aerosol particle mass (Flossmann et al., 1985).

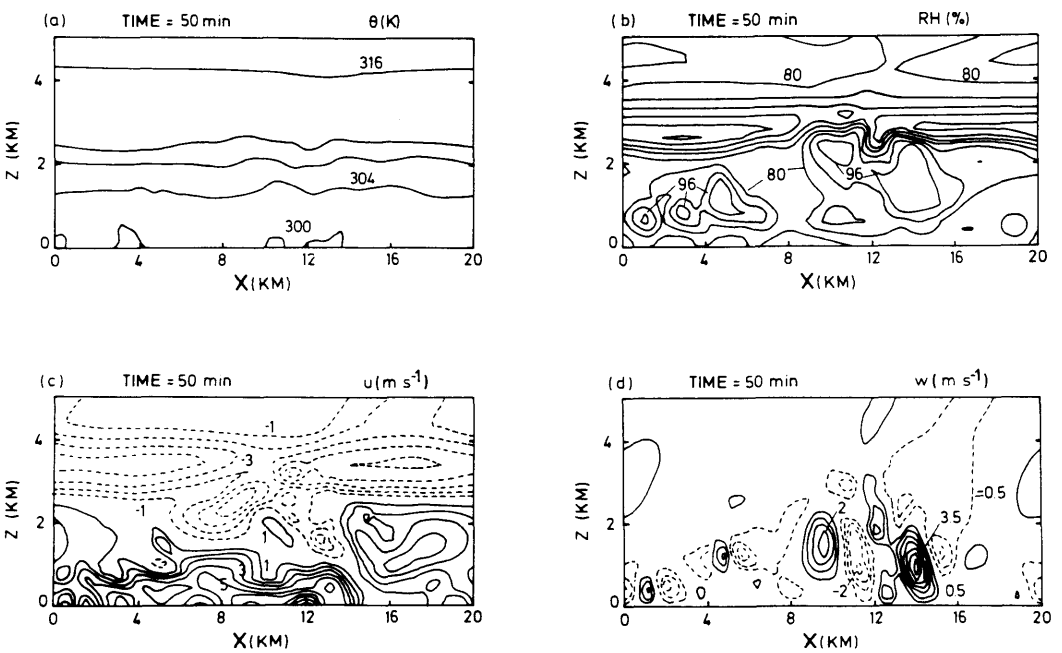

Fig. 4. Distribution of (a) θ, (b) RH, (c) u, and (d) w inside domain at model time $t = 50$ min (corresponds to 24 min after the first cloud formed); with the contour intervals: $\Delta\theta = 4$ K, ΔRH = 8%, $\Delta u = 1$ m/s, $\Delta w = 0.5$ m/s.

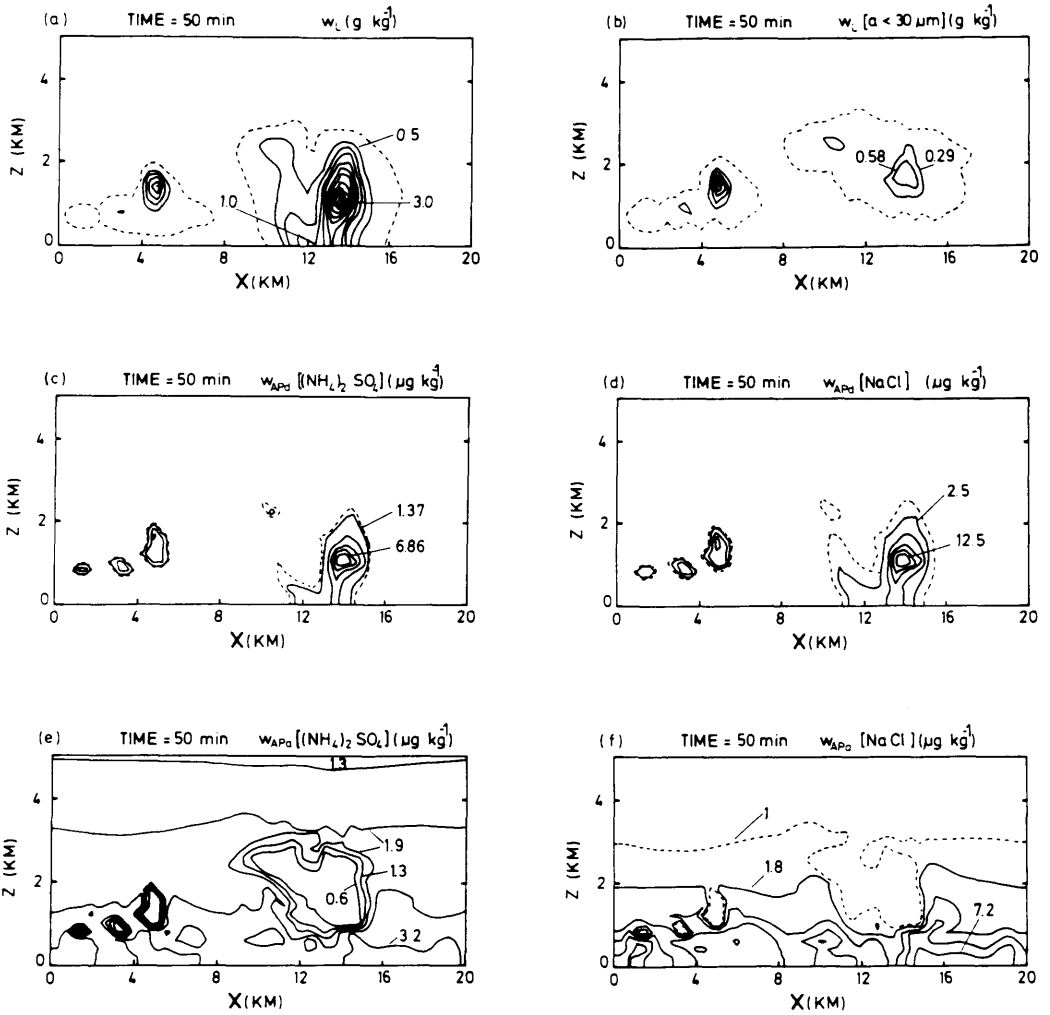

Fig. 5. Distribution of (a) w_L, (b) w_L for drops of $a < 30\ \mu m$, (c) $w_{APd}((NH_4)_2SO_4)$, (d) $w_{APd}(NaCl)$, (e) $w_{APa}((NH_4)_2SO_4)$, (f) $w_{APa}(NaCl)$ inside domain at model time $t = 50$ min (corresponds to 24 min after the first cloud formed); with the contour intervals: $\Delta w_L = 0.25$ g/kg, $\Delta w_L(a < 30\ \mu m) = 0.285$ g/kg, $\Delta w_{APd}((NH_4)_2SO_4) = 1.37\ \mu g/kg$, $\Delta w_{APd}(NaCl) = 2.5\ \mu g/kg$, $\Delta w_{APa}((NH_4)_2SO_4) = 0.645\ \mu g/kg$, $\Delta w_{APa}(NaCl) = 1.77\ \mu g/kg$.

In Fig. 6, a magnification of the field of the relative humidity in the region of the main cloud is given. The dashed curve indicated the contour of the visible cloud. We note from this Figure that large regions with relative humidities as low as 80% exist at the cloud boundaries even though only a homogeneous mixing was considered.

In the course of time the clouds decay and the rain stopped at 70 min of model time. This is when we stopped the calculations. For a summary of the extreme values of the cloud characteristics for the main cloud see Table 2. Also in Table 2 are the corresponding observed values for GATE day 261 as given in the WMO Report (1986). We notice that for all parameters listed the values determined by our simulation compare generally well with those determined by the observations.

In Figs. 7, 8, we have displayed for chosen grid points the evolution of the spectra of the interstitial aerosol particles and the spectra of the drops and

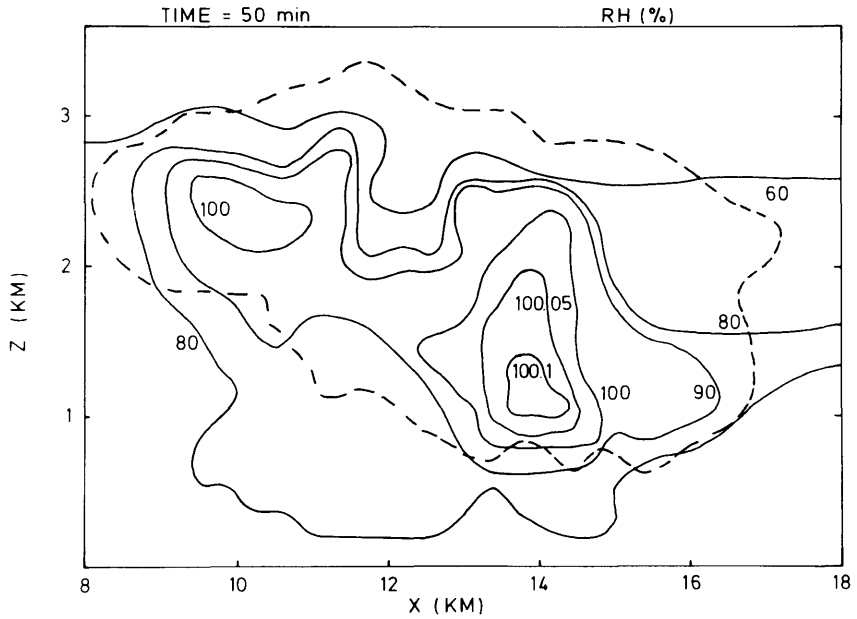

Fig. 6. Magnification of the field of the relative humidity in the region of the main cloud at model time $t = 50$ min (corresponds to 24 min of cloud life time); dashed curve: contours of the visible cloud ($w_L(a < 30\ \mu m) > 0$).

the scavenged aerosol particle mass in the cloud for two different model times and locations near cloud base. In Figs. 7a and 8a the two mass density distribution function for $(NH_4)_2SO_4$ and NaCl in air are displayed. In the first column of these Figures are the spectra at $t = 0$ resulting from the dry spectra of Fig. 2. The spectra are here at equilibrium with the initial ambient relative humidity at the specific grid point. The second column displays the interstitial aerosol particle spectra at 30 and 50 min of model time, resp., at the same grid point at a relative humidity of 100%. The spectra show a cut-off at the larger end due to nucleation scavenging at the same moist aerosol particle radius irrespective of the chemical composition of the particles. This is in agreement with Ahr et al. (1990) who found that the moist cut-off radius due to nucleation scavenging is only dependent on the

Table 2. *Pertinent values for the cloud characteristics (i.e. height of cloud top, diameter of the cloud, maximum relative humidity, maximum updraft velocity, maximum updraft velocity at cloud base, maximum downdraft velocity at cloud base, maximum liquid water content, and average rainrate) at various model times; Last column: observations taken from WMO-Report (1986)*

model time (min)	30	40	50	60	70	observation
cloud life (min)	4	14	24	34	44	-
cloud top (km)	1.4	3	3	2.6	2.6	3
cloud dimension (km)	2.4	4	2 + 3.2	0.6 + 4	4	4
RH_{max} (%)	100.5	102.1	101.4	101.6	101.3	not obs.
w_{max} (m/s)	1.4	10.5	4	2.1	1.0	not obs.
w_{max}(cloud base) (m/s)	1.4	4	4	1.8	0.5	2.5
w_{min}(cloud base) (m/s)	-	-	−2	−0.7	-	−1.6 – −2.8
$w_{L,max}$ (g/kg)	0.2	6.0	3.3	1.3	1.9	1.6
average rain rate (mm/h)	0	0	15	1	0.2	2 – 20

supersaturation and not on the chemical composition of the particles. The total aerosol particle mass is reduced by more than 99% which is in agreement with our earlier work (Flossmann et al., 1985).

In Figs. 7b and 8b, the distributions inside the cloud water are displayed. At model times $t = 30$ min, we notice a narrow drop spectrum and correspondingly a narrow spectrum of aerosol particle mass inside the drops. In Fig. 8b for $t = 50$ min, a bimodal liquid water spectrum has evolved. The mode at the small drop sizes is due to new drops formed by nucleation while the large mode is associated with drops which have been formed by collision and coalescence aloft and are falling towards the ground. Again the aerosol particle mass in the drops experiences a similar behavior. The other two spectra displayed represent the total mixing ratio of material in the drops Q_{APd} and the fraction of $(NH_4)_2SO_4$ in the total scavenged aerosol particle mass. In the mixing ratio Q_{APd} the history of evolution of the drop spectrum is reflected. It displays a maximum at the small particle sizes whenever the supersaturation and the entrainment of particles allows new drops to be nucleated. Then, drops with water masses small as compared to the nucleus mass are introduced into the spectrum. As these drops grow to larger sizes the maximum in the mixing ratio moves with the spectrum until it eventually disappears due to further condensation and collision and coalescence. In Fig. 7b for $t = 30$ min, we notice that particles from the previous nucleation period have already grown to sizes of 10 μm and more, indicating that no few fresh nuclei have been entrained and that the supersaturation has decreased. Thus, for the range between 5 and 10 μm, we notice an increase in the mixing ratio with increasing drop radius as observed by Ogren et al. (1989). In Fig. 8b, for $t = 50$ min, however, a new nucleation period is just going on, introducing new drops with high aerosol particle mixing ratios into the spectrum. Thus, the concentration decreases with radii larger than 5 μm. Therefore, we notice that the evolution of the mixing ratio of aerosol particles in drops is a function of the different age and nucleation time of drops and depends on the entrainment and the evolution of the supersaturation. Thus, we expect that field observations will show mixing ratios which increase or decrease with increasing drop radius.

Also displayed in Fig. 7b and 8b is the fraction of $(NH_4)_2SO_4$ in the aerosol mass scavenged by the drops. We note here that the small drops have a larger fraction of $(NH_4)_2SO_4$ which corresponds to the fact that also the small aerosol particles mainly consist of $(NH_4)_2SO_4$. The larger aerosol particles (> 1 μm), however, consist mainly of NaCl which grow most and are thus in the larger drops. When collision and coalescence starts the aerosol particle mass becomes well mixed in the precipitation sized drops. However, the $(NH_4)_2SO_4$ mass never reaches the value of the NaCl mass, resulting in the fact that the aerosol mass in the precipitation sized drops consists of about 70% NaCl and only 30% $(NH_4)_2SO_4$.

The evolution of the rainfall rate averaged over the whole rainfall region and averaged over 1 min intervals is displayed in Fig. 9a. We notice a maximum rainfall rate of 15 mm/h at 49 min of model time which corresponds to 23 min after the cloud formed. The rain contains scavenged material whose corresponding deposition rate is displayed in Fig. 9b for $(NH_4)_2SO_4$ and NaCl. We notice that the deposition rate of NaCl is significantly larger than that of $(NH_4)_2SO_4$ as expected from Figs. 7b and 8b. In general, we find that the external mixture between sulfate and sea salt particles is reflected in the composition of the rain.

A cross section through the rainfall region is displayed in Fig. 10 for $t = 50$ min of model time. In Fig. 10a, we notice a bimodal distribution in the rainfall rate due to the bifurcation of the cloud itself. The maximum rainfall rate for the considered 5 s interval is over 40 mm/h at $x = 13.4$ km. From Fig. 10b, we notice that the deposition rates of scavenged pollutant mass correspond very closely to the bimodal distribution of the rainfall rate. A look at the pollutant concentration in the rainwater in Fig. 10c shows that for $(NH_4)_2SO_4$ the curve shows only little variation across the rainfall region, while for NaCl we notice two minima in concentration corresponding to the maxima in the rainfall rate. Fig. 10d illustrates the fraction of $(NH_4)_2SO_4$ in the rain water as compared to the total mass of the scavenged material in the rain. We see that the fraction of $(NH_4)_2SO_4$ ranges between 25 and 30% and increases upwind. There the relative humidity (Fig. 6) is lower and consequently the phoretic forces increase resulting in a slightly more efficient impaction scavenging of $(NH_4)_2SO_4$ particles.

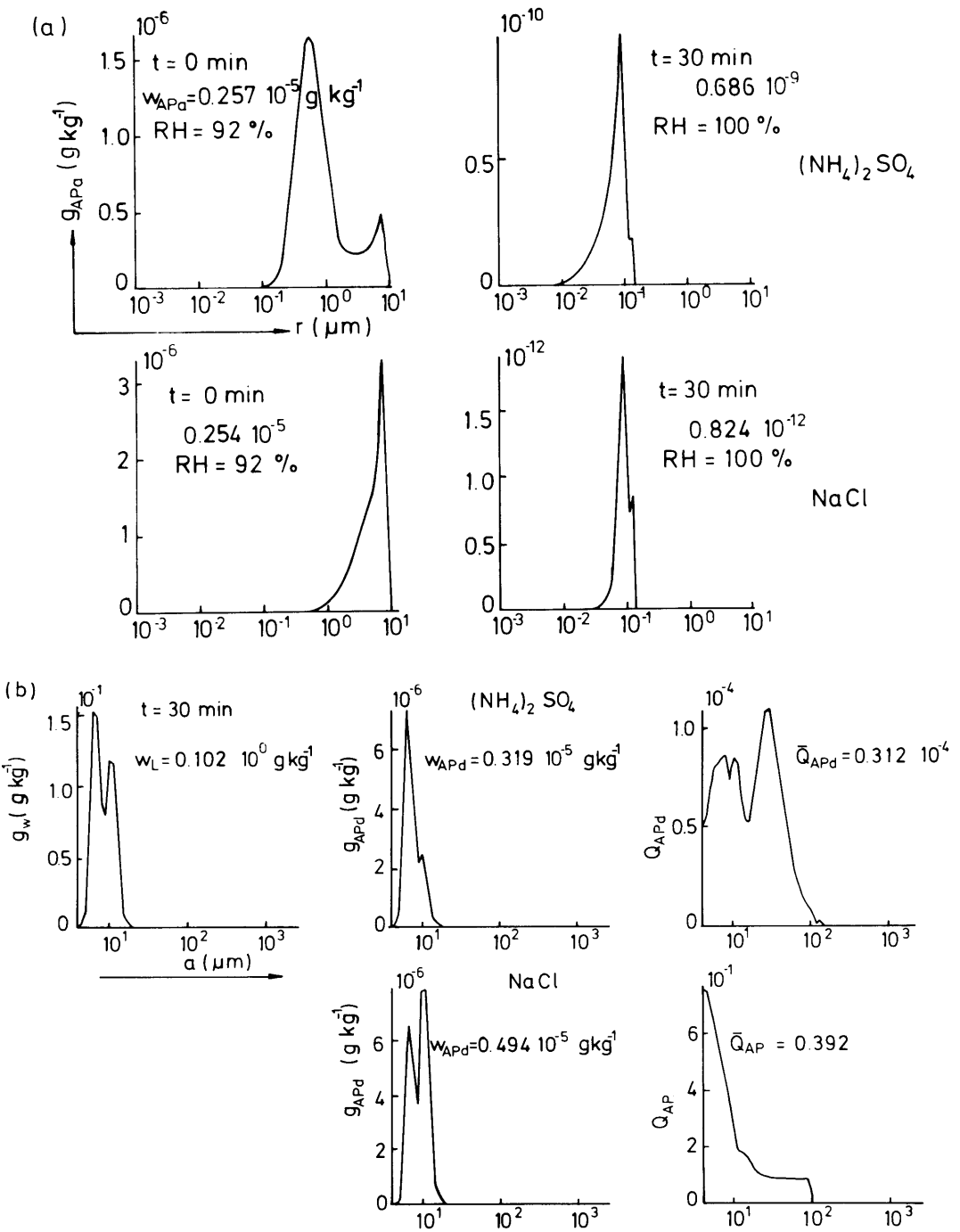

Fig. 7. (a) mass density distribution function $g_{APa}(m_{AP})$ for $(NH_4)_2SO_4$ and NaCl particles at model times $t = 0$ and $t = 30$ min and (b) water mass density distribution function $g_w(m)$, mass density distribution function for $(NH_4)_2SO_4$ and NaCl in the drops $g_{APd}(m)$, mixing ratio of aerosol mass in the drops Q_{APd} and the fraction of $(NH_4)_2SO_4$ compared to the total scavenged aerosol material Q_{AP} at model time $t = 30$ min at $x = 11.8$ km and $z = 1.1$ km.

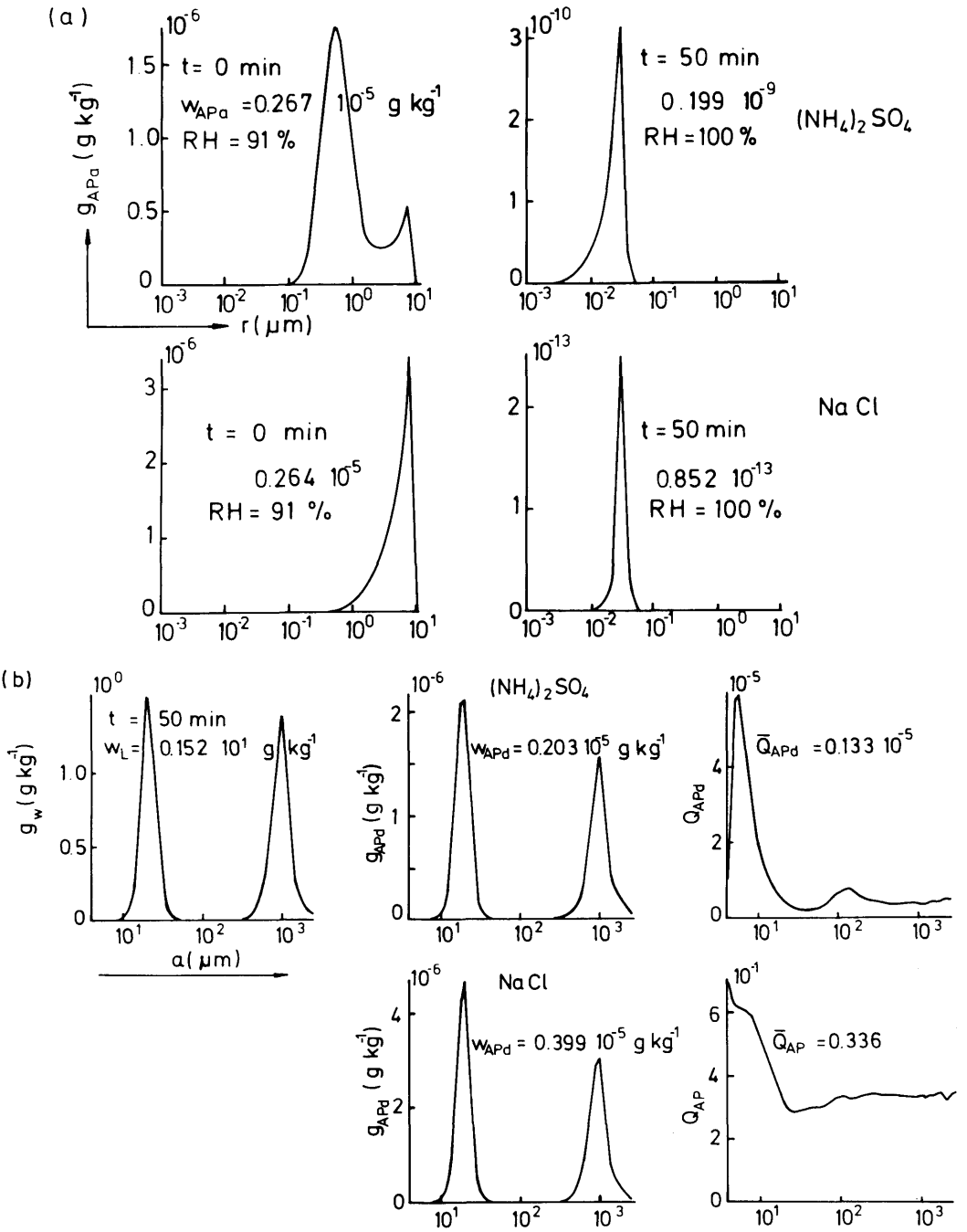

Fig. 8. (a) mass density distribution function $g_{APa}(m_{AP})$ for $(NH_4)_2SO_4$ and NaCl particles in air at model times $t = 0$ and $t = 50$ min and (b) water mass density distribution function $g_w(m)$, mass density distribution function for $(NH_4)_2SO_4$ and NaCl in the drops $g_{APd}(m)$, mixing ratio of aerosol mass in the drops Q_{APd} and the fraction of $(NH_4)_2SO_4$ compared to the total scavenged aerosol material Q_{AP} at model time $t = 50$ min at $x = 13.4$ km and $z = 1.5$ km.

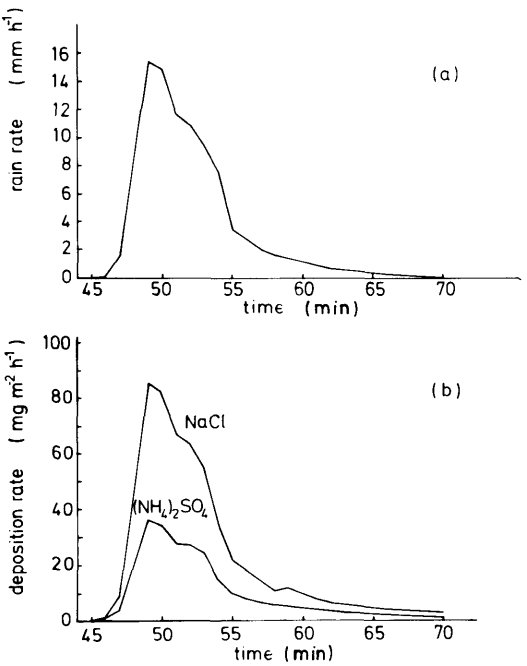

Fig. 9. Evolution of the rainfall rate (a) and the amount of deposited material by the rain (b), averaged over the whole rainfall region and 1 min intervals.

In order to be able to compare our scavenging results with measurements, we plotted in Figs. 11a–e similar information as in Fig. 10 but for a fixed location at the surface at $x = 13.4$ km. The values are averages over 1 min intervals and correspond to the situation where a rain developing cloud moves overhead a fixed location. In Fig. 11c, we notice that the concentration decreases til the maximum of the rainfall rate passed overhead. Then the concentration increases again. Although this behavior is in agreement with observations by Kins (1982) for wet deposition over Europe no field studies are available for comparison with the GATE case. The concentration of sulfate and chloride in the rainwater is in qualitative agreement with values reported by Church et al. (1982), Galloway et al. (1982, 1983), Varhelyi and Gravenhorst (1983), and Parungo et al. (1986b) for the Atlantic at similar latitudes as the GATE domain.

Charlson et al. (1978), Ohta et al. (1985), Winkler (1980, 1983), among others have pointed out that H_2SO_4 particles and their neutralization products with NH_3 are present in the atmosphere as a large family of compounds ranging from H_2SO_4 to $(NH_4)_2SO_4$, a substantial fraction of which consisting of NH_4HSO_4 which in water dissociates into NH_4^+, H^+, and SO_4^{2-}. Water drops containing such particles would therefore become acidic. Unfortunately, exact fractions of the sulfate compounds consisting of NH_4HSO_4 over the oceans are not known. Out of more curiosity, we now wondered what the pH of the rainwater would be if we assumed that the sulfate aerosol considered would not consist of $(NH_4)_2SO_4$ particles but instead entirely of NH_4HSO_4 particles. For this case we found that the pH of the rainwater across the rainfall region assumed a value of 4.7 which happens to lie within the range observed, e.g., by Galloway et al. (1982) and Parungo et al. (1986b). We may conclude from this that, in order to account for the pH in marine precipitation no gas scavenging is necessary if the sulfate would be completely in the form of NH_4HSO_4 particles. However, we are aware of the fact that the agreement between our computed and the observed values is merely coincidental since the pH of marine rain water is not only affected by the sulfate compound but also in a complicated way by the alkalinity of the sea salt aerosol and by possibly ongoing gas scavenging and subsequent oxidation in the liquid phase.

In Table 3, we have computed values for four

Table 3. *Precipitation and scavenging efficiencies for the different species of aerosol particles considered as defined by Eq. (8), 3rd column: results from this paper, 4th column: results for the Hawaiian cloud simulated by Flossmann and Pruppacher (1988)*

		GATE 261	Hawaii case
E_1		46%	12%
E_2	$(NH_4)_2SO_4$	93%	95%
	NaCl	85%	-
	total	87%	95%
E_3	$(NH_4)_2SO_4$	34%	14%
	NaCl	43%	-
	total	40%	14%
E_4	$(NH_4)_2SO_4$	22%	40%
	NaCl	36%	-
	total	32%	40%

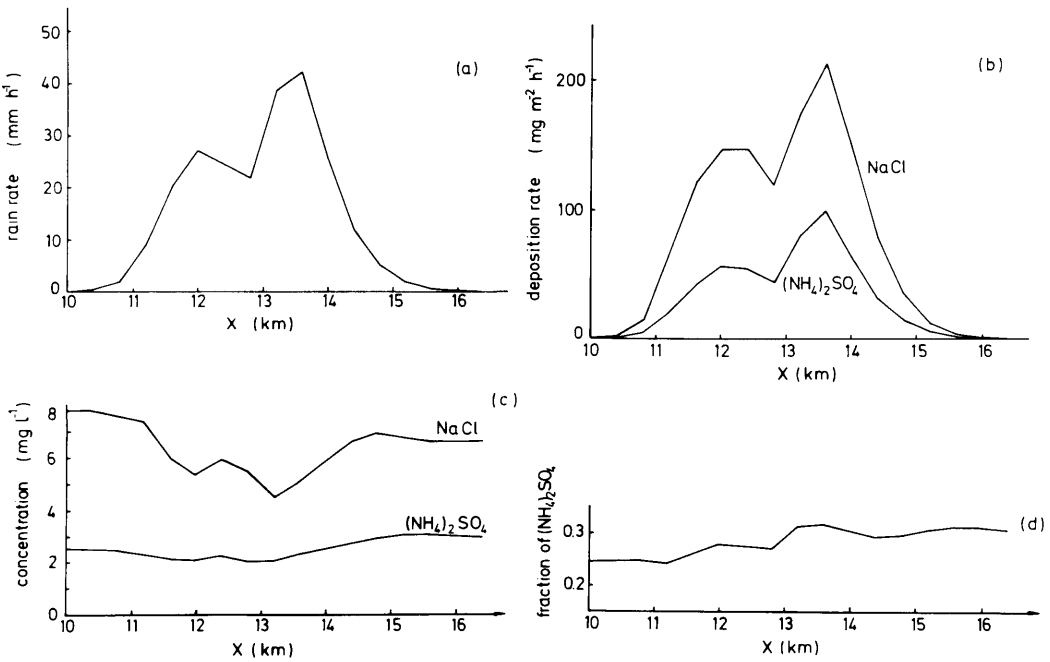

Fig. 10. Cross section through the rainfall rate (a), the amount of deposited material by the rain (b), the concentration of scavenged material in the rain (c), and the percentage of $(NH_4)_2SO_4$ in the total deposited material (d) at model time $t = 50$ min for a 5-s interval.

specific efficiencies pertaining to the end time of our computation as:

$$E_1 = \frac{\text{cumulative rain mass on the ground}}{\text{cumulative water mass converted from the vapor}}$$

$$E_2 = \frac{\text{cumulative nucleation scavenging}}{\text{cumulative aerosol mass scavenged by nucleation and impaction}}$$

$$E_3 = \frac{\text{cumulative aerosol particle mass in rain}}{\text{cumulative aerosol mass scavenged by nucleation and impaction}}$$

$$E_4 = \frac{\text{cumulative impaction scavenging}}{\text{cumulative aerosol particle mass in rain}} \quad (8)$$

Also displayed in this table are the efficiencies as computed by Flossmann and Pruppacher (1988) for a stationary Hawaiian cloud. In contrast to the present model run the aerosol particles in the Hawaiian case were assumed to consist uniformly of 10% $(NH_4)_2SO_4$ and 90% insoluble silicate as an air/land trajectory was assumed. We notice from Table 3 that the two clouds considered have quite different precipitation efficiencies. It is important here to note that in both cases the scavenging efficiency E_3 behaves in close correspondance to E_1. The major amount of pollutant mass is incorporated into the cloud water through nucleation scavenging ($85\% < E_2 < 95\%$) as already suggested by Flossmann and Pruppacher (1988). E_2 for NaCl is in the GATE case smaller than E_2 for $(NH_4)_2SO_4$. At first this seems surprising, since NaCl is prominently found in the large aerosol particles which grow to larger sizes more quickly. But these particles are also more efficiently scavenged by impaction below cloud base due to the high impaction efficiencies in this size range. This is, e.g., reflected in the values for E_4. E_4 gives the % of aerosol particles scavenged by impaction as compared to the total material deposited on the ground by precipitation. This fraction is larger for the Hawaiian case than for the GATE case since the contribution from nucleation

Tellus B/43/3-4

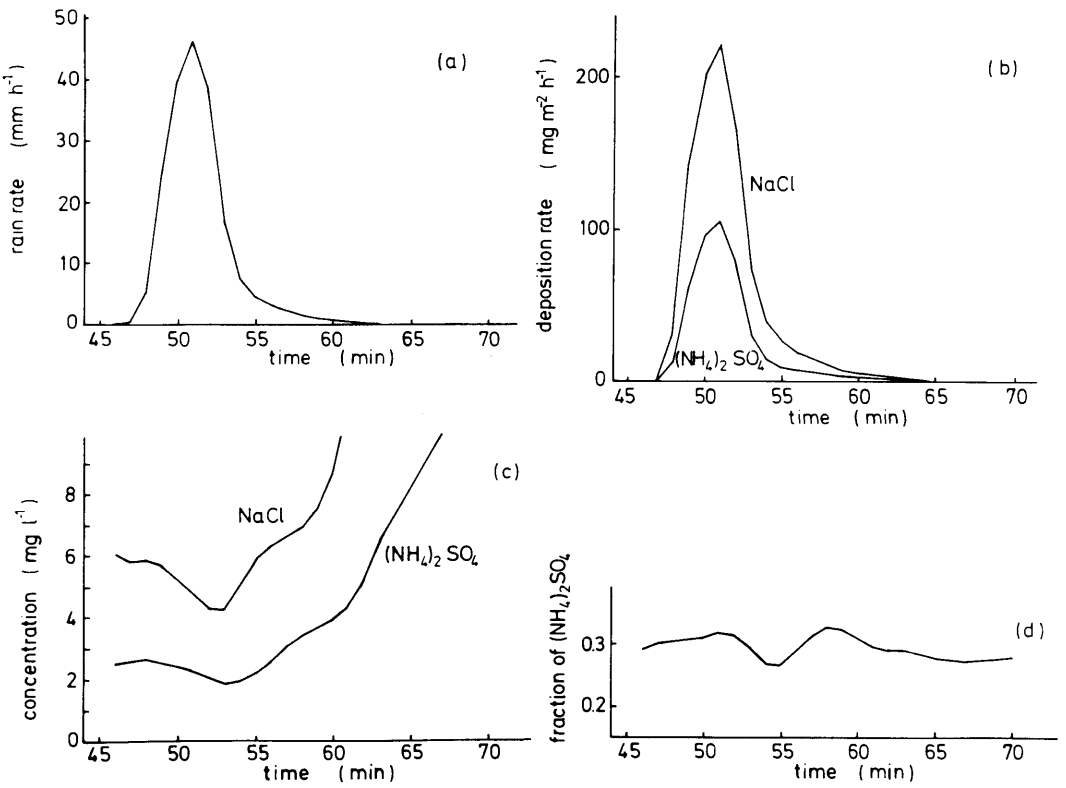

Fig. 11. Evolution of the rainfall rate (a), the amount of deposited material by the rain (b), the concentration of scavenged material in the rain (c), and the % of $(NH_4)_2SO_4$ in the total deposited material (d) at 13.4 km averaged over 1-min intervals.

scavenging to the aerosol material in the rain on the ground is smaller due to the low precipitation efficiency. Since we have shown (Flossmann et al., 1985) that impaction scavenging plays only a negligible role inside the cloud we can safely assume that the fraction E_4 is almost exclusively taken up below the cloud. If we assume, in addition, that little of this scavenged material is lost due to complete evaporation of the drops we can conclude that for the cases studied 20–40% of the aerosol material in the rain is scavenged below cloud base. The different values for the impaction scavenging E_4 are also responsibel for the fact that for the Hawaiian case the scavenging efficiency E_3 is slightly higher than the precipitation efficiency E_1 in contrast to the GATE case.

For parameterisation of scavenging by cumulus clouds in larger scale models the total processed material involved in these processes might be of

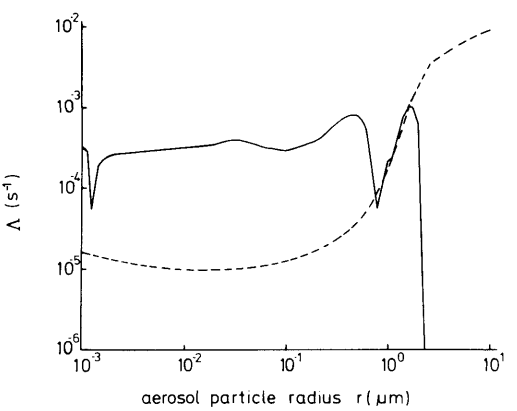

Fig. 12. Scavenging coefficient Λ_A (eq. 9) as a function of aerosol particle radius for the time period between 45 and 55 min of model time at $x = 13.4$ km at the surface; dashed curve: Λ_B resulting from eq. (10).

interest. Our model, however, is only two-dimensional and thus the total amounts only correspond to a "slice" of cloud. Assuming that the values in this "slice" of cloud are the same ones all over a 3-D cloud with a mean diameter of 5 km we have roughly calculated the total material processed by the cloud. The results of this estimate are summarized in Table 4.

The spectral scavenging coefficient Λ_A which is defined as the reduction in the aerosol particle spectrum during a rain event,

$$\Lambda_A = -\frac{1}{f_{APa}(m_{AP})} \frac{\partial f_{APa}(m_{AP})}{\partial t} \tag{9}$$

is displayed in Fig. 12 for our model case for the variation in the aerosol particle spectrum at the ground. The scavenging coefficient, which refers to the model time interval between 45 and 55 min where the main rain is falling (see Fig. 11a), assumes values near 10^{-4} with little variation over the aerosol particle size spectrum. Below cloud scavenging coefficients of this order of magnitude have been observed during field studies by Davenport and Peters (1978) and Schumann (1989). These authors attempted to interpret their measurements in terms of the scavenging coefficient:

$$\Lambda_B = \int_0^\infty K_{AP}(m_{AP}, m)\, f_d(m)\, dm \tag{10}$$

with the collection kernel

$$K_{AP}(m_{AP}, m) = E_{AP}(m_{AP}, m)\, \pi(a+r)^2\, V_\infty(m) \tag{11}$$

to be computed from theoretically derived and experimentally verified collection efficiencies, under the assumption that one may set $\Lambda_A = \Lambda_B$. With their observed raindrop spectra and the values for the collection efficiencies as published, e.g., by Grover et al. (1977) and Wang et al. (1978) they found Λ_B values which were at least one order of magnitude smaller than the observed Λ_A values. Since they assumed that Λ_A should be equal to Λ_B they suggested that other impaction scavenging mechanisms not yet considered in the collection efficiencies or improperly determined values for the collection efficiencies would account for this discrepancy. In order to shed light on this problem, we have plotted the same coefficients for the resulting drop spectrum at 50 min in Fig. 12 and have encountered indeed the same discrepancy between Λ_A and Λ_B. However, since in the present model the *same* collection efficiencies have been used for eq. (9) as well as (10) it becomes obvious that the reason for the discrepancy between Λ_A and Λ_B does not lie in the

Table 4. *Total material processed by the cloud estimated from 2-D simulation, 3rd column: results from this paper, 4th column: results for the Hawaiian cloud simulated by Flossmann and Pruppacher (1988)*

		GATE 261	Hawaii case
total condensation		9200 t	14000 t
total rain on ground		4200 t	1600 t
nucleation scavenging	$(NH_4)_2SO_4$	300 kg	290 kg
	NaCl	490 kg	-
	total	790 kg	2900 kg
impaction scavenging	$(NH_4)_2SO_4$	24 kg	15 kg
	NaCl	90 kg	-
	total	114 kg	150 kg
aerosol particles in rain	$(NH_4)_2SO_4$	110 kg	43 kg
	NaCl	250 kg	-
	total	360 kg	430 kg

values for the collection efficiencies. Looking more closely at eq. (2), we can see that

$$\Lambda_A = -\frac{1}{f_{APa}(m_{AP})}\frac{\partial f_{APa}(m_{AP})}{\partial t}$$
$$= \frac{1}{f_{APa}(m_{AP})}\nabla\cdot[\boldsymbol{v} f_{APa}(m_{AP})]$$
$$-\frac{1}{f_{APa}(m_{AP})}\nabla\cdot[K_m\nabla f_{APa}(m_{AP})]$$
$$-\frac{1}{f_{APa}(m_{AP})}\frac{\partial f_{APa}(m_{AP})}{\partial t}\bigg|_{act}$$
$$-\frac{1}{f_{APa}(m_{AP})}\frac{\partial f_{APa}(m_{AP})}{\partial t}\bigg|_{con/eva}$$
$$-\frac{1}{f_{APa}(m_{AP})}\frac{\partial f_{APa}(m_{AP})}{\partial t}\bigg|_{AP,coll}$$
$$= \frac{1}{f_{APa}(m_{AP})}\nabla\cdot[\boldsymbol{v} f_{APa}(m_{AP})]$$
$$-\frac{1}{f_{APa}(m_{AP})}\nabla\cdot[K_m\nabla f_{APa}(m_{AP})]$$
$$-\frac{1}{f_{APa}(m_{AP})}\frac{\partial f_{APa}(m_{AP})}{\partial t}\bigg|_{act}$$
$$-\frac{1}{f_{APa}(m_{AP})}\frac{\partial f_{APa}(m_{AP})}{\partial t}\bigg|_{con/eva}$$
$$+\Lambda_B, \qquad (12)$$

where the term AP, coll is identical to Λ_B (see Flossmann et al., 1985). Thus, $\Lambda_A = \Lambda_B$ *only* if the other terms in eq. (12) are zero or so small that they can be neglected as compared to the others. This is certainly true for the activation term which plays no role below cloud. Although it might be true over limited time intervals for advection and turbulent mixing, it is certainly not true for the term con/eva in eq. (12) due to changes in the aerosol particle sizes caused by humidity variations at the considered location:

$$\Lambda_A \approx -\frac{1}{f_{APa}(m_{AP})}\frac{\partial f_{APa}(m_{AP})}{\partial t}\bigg|_{con/eva}$$
$$+\Lambda_B. \qquad (13)$$

In order to estimate this effect, we have set $\Lambda_B = 0$ and imposed a small fixed humidity increase of only 1% from 73% to 74%. Applying eq. (13) a spectral scavenging coefficient Λ_A of about $5\cdot10^{-5}$ already resulted from the growth of the aerosol particle spectrum to larger size categories masking the fact that not a single aerosol particle was actually scavenged by the drops. A further indication that the difference between Λ_A and Λ_B is due to the diffusional growth process is the fact that the Λ_A vaues for NaCl alone differ by a factor of 3 from the Λ_A for $(NH_4)_2SO_4$ alone. Also a result of the condensation process is that in Fig. 12, Λ_A appears to be zero for aerosol particles $r > 2.5$ μm. This is due to a negative scavenging coefficient from an increase of the number of large particles by condensation. Λ_B, however, increases with larger aerosol particle sizes due to the increased collection efficiency. The entire form of the scavenging coefficient curve Λ_A in Fig. 12, as resulting from the actual humidity variations in the present model, depends on the shape of the original aerosol particle spectrum, the chemical composition of the particles and the humidity changes. This effect adds significantly to the effect of impaction scavenging alone. The fact that the scavenging coefficient has often been found to be rather independent of aerosol particle size may be attributed to a well mixed aerosol of different composition (Davenport and Peters, 1978). Less well mixed aerosols may lead to spectral scavenging coefficients with maxima and minima (Schumann, 1989). Not included in our model calculation were effects of electric charges on the scavenging process. Wang et al. (1978), Wang and Pruppacher (1977), and Barlow and Latham (1983), among others, have shown that electric charges on drops and aerosol particles result in an increase of the scavenging efficiency by at most one order of magnitude in the aerosol particle size range between 10^{-2} and 1 μm. Thus, electric effects may also have added to the discrepancies between the Λ_A and Λ_B values as observed by Davenport and Peters (1978) and Schumann (1989). Our scavenging coefficient as given in Fig. 12, however, were both derived disregarding electric effects. As the discrepancy between Λ_A and Λ_B was still encountered in the same magnitude as observed, we can conclude that electric effects might add to this discrepancy, however, cannot be solely responsible.

5. Summary and conclusions

Our 2-D dynamic model including spectral microphysics and scavenging has been evaluated

for a warm precipitating convective cloud at Day 261 (18 September 1974) of the GATE campaign. After 19 min of life time the cloud precipitated. Two different chemical species ($(NH_4)_2SO_4$ and NaCl) of aerosol particles were followed in the air, inside the drops in the cloud, and inside the drops reaching the ground. Concerning the dynamics and microphysics, as well as the scavenging and wet deposition in a marine air mass the model results agree quite well with the available observations. Furthermore, they are consistent with the results from our earlier papers (Flossmann and Pruppacher, 1988; Ahr et al., 1990). From the present results and the results of an earlier paper (Flossmann and Pruppacher, 1988) rough estimates are derived for the total material processed by such warm convective clouds as input for larger scale models. In particular this study allowed the following conclusions for the situation considered.

- If a drop spectrum forms on an aerosol spectrum where the small particles consist of $(NH_4)_2SO_4$ and the large ones of NaCl, the resulting small drops also mainly consist of $(NH_4)_2SO_4$ and the larger drops of NaCl. One would expect that collision and coalescence eliminates this difference in the raindrops. However, it only causes a redistribution of the chemical species such that the precipitation sized drops evenly consist of NaCl to about 70%.
- The mixing ratio of aerosol material in drops is a function of the age of the drops and the history of their evolution and therefore the variation of the mixing ratio depends on the entrainment of aerosol particles and the time and space evolution of the relative humidity. The mixing ratio decreased with increasing drop radius at almost all grid points due to continuous activation of fresh particles. However, if no new drops were activated the mixing ratio for the small drops also increased with increasing drop radius.
- Assuming that the sulfate aerosol would not consist of $(NH_4)_2SO_4$ particles but instead consist of NH_4HSO_4 particles the acidic cloud water assumes a pH of 4.7 which agrees with observed pHs in precipitating clouds of marine air masses. Thus, to explain these observed pHs acidic sulfate particles suffice. However, the pH of marine rain water is not only determined by the sulfate compound but also by the alcalinity of the sea salt aerosol particles and by ongoing gas scavenging and subsequent oxidation in the liquid phase.
- The scavenging efficiency of a convective warm cloud is closely related to the precipitation efficiency of the cloud. For the presently considered storm the precipitation efficiency was 46%, while the overall scavenging efficiency was 40%, 34% for $(NH_4)_2SO_4$ and 43% for NaCl. The major amount of pollutant mass (87%, 93% for $(NH_4)_2SO_4$ and 85% for NaCl) is incorporated into the cloud water through nucleation scavenging. 32% of the overall aerosol material in the rain at the ground (22% for $(NH_4)_2SO_4$ and 36% for NaCl), however, was scavenged below cloud base.
- The spectral scavenging coefficient for the presently considered storm was on the order of 10^{-4}. The differences between two commonly used formulations for calculating the scavenging coefficient Λ can be explained in terms of humidity fluctuations in the sub-cloud air.

6. Acknowledgements

The author wants to thank Professor Dr. H. R. Pruppacher for his scientific advice, helpful discussion, and his support in preparing the manuscript. Thus, the author dedicates this paper to Professor Dr. H. R. Pruppacher on the occasion of his 60th birthday. The author also acknowledges with gratitude Professor Dr. U. Schumann of the DLR for helping to arrange for computer time on the CRAY X-MP/216 at the DLR Oberpfaffenhofen, FRG. This research was funded by the Ministry for Research and Technology of the Federal Republic of Germany under project 325-4007-0704580. The author of this paper is solely responsible for its content. The author also acknowledges with gratitude the financial support of the German National Science Foundation under Project SFB 233.

REFERENCES

Ahr, M., Flossmann, A. I. and Pruppacher, H. R. 1990. On the effect of the chemical composition of atmospheric aerosol particles on nucleation scavenging and the formation of a cloud interstitial aerosol. *J. Atmos. Chem. 9*, 465–478.

Ayers, G. P. and Larson, T. V. 1990. Numerical study of

droplet size dependent chemistry in oceanic, wintertime stratus cloud at southern mid-latitudes. *J. Atmos. Chem. 11*, 143–167.

Baker, M. B., Corbin, R. G. and Latham, J. 1980. The influence of entrainment on the evolution of cloud droplet spectra: I. A model of inhomogeneous mixing. *Quart. J. Roy. Met. Soc. 106*, 581–598.

Baker, M. B. and Latham, J. 1982. A diffusive model of the turbulent mixing of dry and cloudy air. *Quart. J. Roy. Met. Soc. 108*, 871–898.

Barlow, A. K. and Latham, J. 1983. A laboratory study of the scavenging of sub-micron aerosol by charged raindrops. *Quart. J. Roy. Met. Soc. 109*, 763–770.

Blanchard, D. C. and Woodcock, A. H. 1980. The production, concentration, and vertical distribution of sea salt aerosol. *Ann. N.Y. Acad. Sci. 338*, 330–347.

Charlson, R. J., Covert, D. S., Larson, T. V. and Waggoner, A. P. 1978. Chemical properties of tropospheric sulfar aerosols. *Atmos. Environ. 12*, 39–53.

Church, T. M., Galloway, J. N., Jickells, T. D. and Knap, A. H. 1982. The chemistry of western atlantic precipitation at the mid-atlantic coast and on Bermuda. *J. Geophys. Res. 87*, 11013–11018.

Clark, T. L. 1977. A small scale dynamic model using a terrain-following coordinate transformation. *J. Comput. Phys. 24*, 186–215.

Clark, T. L. 1979. Numerical simulations with a three dimensional cloud model. *J. Atmos. Sci. 36*, 2191–2215.

Clark, T. L. and Gall, R. 1982. Three dimensional numerical model simulations of air flow over mountainous terrain: A comparison with observation. *Mon. Wea. Rev. 110*, 766–791.

Clark, T. L. and Farley, R. D. 1984. Severe downslope windstorm calculations in two and three spatial dimensions using anelastic interactive grid nesting. *J. Atmos. Sci. 41*, 329–350.

Daum, P. H., Schwartz, S. E. and Newman, L. 1983. Studies of gas and aqueous phase composition of stratiform clouds. *Precipitation scavenging, dry deposition and resuspension 1*, Elsevier, 31–52.

Davenport, H. M. and Peters, L. K. 1978. Field studies of atmospheric particulate concentration changes during precipitation. *Atmos. Environ. 12*, 997–1008.

Flossmann, A. I. 1987. *A theoretical investigation of the removal of atmospheric trace constituents by means of a dynamic model.* Ph.D. Thesis. Meteorological Institute, Johannes Gutenberg Universität, Mainz, FRG (available from University of Mainz), 186 pp.

Flossmann, A. I., Hall, W. D. and Pruppacher, H. R. 1985. A theoretical study of the wet removal of atmospheric pollutants. Part I: The redistribution of aerosol particles captured through nucleation and impaction scavenging by growing cloud drops. *J. Atmos. Sci. 42*, 582–606.

Flossmann, A. I. and Pruppacher, H. R. 1988. A theoretical study of the wet removal of atmospheric pollutants. Part III: The uptake, redistribution and deposition of $(NH_4)_2SO_4$ particles by a convective cloud using a two-dimensional cloud dynamics model. *J. Atmos. Sci. 45*, 1857–1871.

Galloway, J. N., Likens, G. E., Keene, W. C. and Miller, J. M. 1982. The composition of precipitation in remote areas of the world. *J. Geophys. Res. 87*, 8771–8786.

Galloway, J. N., Knap, A. H. and Church, T. M. 1983. The composition of Western Atlantic Precipitation using shipboard Collectors. *J. Geophys. Res. 88*, 10859–10864.

Grover, S. M., Pruppacher, H. R. and Hamiliec, A. E. 1977. A numerical determination of the efficiency with which spherical aerosol particles collide with spherical water drops due to inertial impaction and phoretic and electric forces. *J. Atmos. Sci. 34*, 1655–1663.

Hall, W. D. 1980. A detailed microphysical model within a two-dimensional dynamic framework: Model description and preliminary results. *J. Atmos. Sci. 37*, 2486–2507.

Hegg, D. A. and Hobbs, P. V. 1982. Measurements of sulfate production in natural clouds. *Atmos. Environ. 16*, 2663–2668.

Hill, T. A. and Choularton, T. W. 1986. A model of the development of the droplet spectrum in a growing cumulus turret. *Quart. J. Roy. Met. Soc. 112*, 531–554.

Jaenicke, R. 1988. Aerosol physics and chemistry. In: Landolt-Boernstein: *Zahlenwerte und Funktionen aus Naturwissenschaften und Tecknik, V 4b*, G. Fisher, Editor, Springer, 391–457.

Kins, L. 1982. The variation of chemical composition of rainwater during individual precipitation events. *Deposition of atmospheric pollutants*, Reidel, 87–96.

Lazrus, A. L., Haagenson, P. L., Koh, G. L., Huebert, C. W., Kreitzberg, K. C. W., Likens, G. E., Mohnen, U. A., Wilson, W. E. and Winchester, J. W. 1983. Acidity in air and water in the case of warm-frontal precipitation. *Atmos. Environ. 17*, 581–592.

Leaitch, W. R., Strapp, J. W., Wiebe, H. A. and Isaac, G. A. 1983. Measurements of scavenging and transformation of aerosol inside cumulus. *Precipitation Scavenging, Dry Deposition and Resuspension 1*, Elsevier, 53–70.

Lilly, D. K. 1962. On the numerical simulation of buoyant convection. *Tellus 14*, 148–172.

Lovett, R. F. 1978. Quantitative measurements of airborne sea-salt in the north atlantic. *Tellus 30*, 358–364.

Murakami, M., Kimura, T., Magono, C. and Kikuchi, K. 1983. Observations of precipitation scavenging for water soluble particles. *J. Meteor. Soc. Japan 61*, 346–357.

Ogren, J. A., Heintzenberg, J., Zuber, A., Noone, K. J. and Charlson, R. J. 1989. Measurements of the size-dependence of solute concentrations in cloud droplets. *Tellus 41B*, 24–31.

Ohta, S., Okita, T. and Kusaka, F. 1985. Measurement of atmospheric sulfuric acid particles using diazomethane methylation. *J. Meteor. Soc. Japan 63*, 112–118.

Parungo, F. P., Nagamoto, C. T., Rosinski, J. and Haagenson, P. L. 1986a. A study of marine aerosols over the pacific ocean. *J. Atmos. Chem. 4*, 199–226.

Parungo, F. P., Nagamoto, C. T. and Harris, J. M. 1986b. Temporal and spatial variations of marine aerosols over the atlantic ocean. *Atmospheric Research 20*, 23–37.

Prodi, F., Santachiara, G. and Oliosi, F. 1983. Characterization of aerosols in marine environments (mediterranean, red sea, and indian ocean). *J. Geophys. Res. 88*, 10957–10968.

Radke, L. 1983. Preliminary measurements of the size distribution of cloud interstitial aerosol. *Precipitation Scavenging, Dry Deposition and Resuspension 1*, Elsevier, 71–78.

Roesner, S., Flossmann, A. I. and Pruppacher, H. R. 1990. The effect of pre-conditioning of air by successive convective elements on the evolution of the drop spectrum in clouds. *Quart. J. Roy. Met. Soc.* in press.

Scott, B. C. and Laulainen, N. S. 1979. On the concentration of sulphate in precipitation. *J. Appl. Meteor. 18*, 138–147.

Simpson, J., Helvoirt, G. V. and McCumber, M. 1982. Three-Dimensional Simulation of Cumulus Congestus Clouds on GATE Day 261. *J. Atmos. Sci. 39*, 126–145.

Schumann, T. 1989. *Precipitation scavenging of aerosol particles: a winter-time field study*. Ph.D. Thesis (available from ETH Zurich, Switzerland), 293 pp.

Schumann, T., Zinder, B. and Waldvogel, A. 1988. Aerosol and hydrometeor concentrations and their chemical composition during winter precipitation above a mountain slope. *Atmos. Environ. 22*, 1443–1459.

Smagorinsky, J. 1963. General circulation experiments with the primitive equations: 1. Basic experiment. *Mon. Wea. Rev. 91*, 99–164.

Smolarkiewicz, P. K. and Clark, T. L. 1985. Numerical simulation of the evolution of a three dimensional field of cumulus clouds. Part I: Model description, comparison with observations and sensitivity studies. *J. Atmos. Sci. 42*, 502–522.

Turpeinen, O. and Yau, M. K. 1981. Comparison of results from a three-dimensional cloud model with statistics of radar echoes on day 261 of GATE. *Mon. Wea. Rev. 109*, 1495–1511.

Twohy, C. H., Austin, P. H. and Charlson, R. J. 1989. Chemical consequences of the initial diffusional growth of cloud droplets: a clean marine case. *Tellus 41B*, 51–60.

Varhelyi, G. and Gravenhorst, G. 1983. Production rate of airborne sea-salt sulfar deduced from chemical analysis of marine aerosols and precipitation. *J. Geophys. Res. 88*, 6737–6751.

Wang, P. K. and Pruppacher, H. R. 1977. An experimental determination of the efficiency with which aerosol particles are collected by water drops in subsaturated air. *J. Atmos. Sci. 34*, 1664–1669.

Wang, P. K., Grover, S. N. and Pruppacher, H. R. 1978. On the effect of electric charges on the scavenging of aerosol particles by cloud and small rain drops. *J. Atmos. Sci. 35*, 1735–1743.

Winkler, P. 1980. Observations on acidity in continental and in marine atmospheric aerosols and in precipitation. *J. Geophys. Res. 85*, 4481–4486.

Winkler, P. 1983. Acidity of aerosol particles and of precipitation in the north polar region and over the atlantic. *Tellus 35B*, 25–30.

WMO Weather modification research programme, 1986. Report of the *International Cloud Modeling Workshop/ Conference Irsee*, FRG, 15–19 July, 1985, Technical Document WMO/TD-No. 139, WMO Report No. 8.

Wolff, G. T., Ruthkosky, M. S., Stroup, D. S., Korsog, P. E., Ferman, M. A., Wendel, G. J. and Stedman, D. H. 1986. Measurements of SO_x, NO_x and aerosol species on Bermuda. *Atmos. Environ. 20*, 1229–1239.